Fibers and Polymers 2015, Vol.16, No.9, 2021-2027
DOI 10.1007/s12221-015-5479-3

ISSN 1229-9197 (print version)
ISSN 1875-0052 (electronic version)

Electrical and Dielectric Properties of Poly(1,3,4-oxdiazole) Nanocomposite Films with Graphene Sheets Dispersed in Layers

Eunbin Lee and Young Gyu Jeong*

Department of Advanced Organic Materials and Textile System Engineering, Chungnam National University, Daejeon 34134, Korea

(Received June 23, 2015; Accepted July 4, 2015)

Abstract: Electrical and dielectric measurements over a broad frequency range from 20 Hz to 2 MHz were carried out for a series of sulfonated poly(1,3,4-oxadiazole) (sPOD) nanocomposite films containing exfoliated graphene sheets of 0.1-10.0 wt%, which were manufactured via ultrasonication-based solution mixing and casting method. TEM and XRD data revealed that the graphene sheets were dispersed by forming a layered structure in the nanocomposite films with >2.0 wt% graphene. The frequency-dependent electrical conductivity and relative permittivity of the nanocomposite films were dependent on the graphene content. The neat sPOD and its nanocomposites with lower graphene contents of 0.1-2.0 wt% exhibited low electrical conductivity of ~10^{-13}-10^{-12} S/cm and relative permittivity of 1.7-6.6 at 20 Hz. In cases of the nanocomposite films with high graphene contents of 5.0 and 10.0 wt%, highly improved relative permittivity of ~101 and ~560 at 20 Hz as well as electrical conductivity of ~10^{-9} S/cm and ~10^{-6} S/cm was attained at 20 Hz, respectively. In addition, the nanocomposite films with 5.0 and 10.0 wt% exhibited relatively high capacitance of ~39.7 pF and ~75.5 pF at 20 Hz, respectively. The highly enhanced relative permittivity and capacitance for the nanocomposite films with 5.0-10.0 wt% graphene was interpreted to be owing to the accumulation of electronic charges at the interfaces between insulating sPOD matrix and conductive graphene sheets dispersed in layers.

Keywords: Poly(1,3,4-oxadiazole), Graphene, Nanocomposite films, Dielectric property, Electrical property

Introduction

Materials with high relative permittivity or dielectric constant are widely applied in electronic and electromechanical systems, such as embedded capacitors in microelectronics, electromagnetic interference shielding and energy storage devices. Many ceramic-, metal- and polymer-based composites have been investigated to obtain high relative permittivity. Among them, polymer composites are most widely studied due to their easy processing, flexibility, high dielectric strengths and superior environmental resistance [1,2]. For polymer composites with high relative permittivity, ceramic or carbon nanomaterials have been chosen as high dielectric reinforcing fillers. In cases of the polymer composites containing ceramic additives such as $BaTiO_3$ and PZT, dielectric properties can be enhanced significantly, but large volume fraction is often required, which leads to deteriorate the mechanical properties and dielectric strengths of the composites [3,4]. On the other hand, carbon nanomaterials such as carbon nanotubes, graphene and their derivatives with unique low dimensional structures as well as excellent mechanical, electrical, and thermal properties [5-8], have been also chosen as functional nanofillers for high dielectric polymer nanocomposites [2,9,10].

Aromatic polymers containing oxadiazole units are known to have excellent thermal stability, chemical resistance, and hydrolytic stability, in addition to their facile processibility to form fibers, films, coating, felts, laminates, and membranes [11-13]. Also oxadiazole-based polymers have recently attracted attention as polymer light-emitting diodes, acid sensor, electron and proton conducting materials due to their aromatic and basic characteristics of the oxadiazole ring [14]. Aromatic poly(1,3,4-oxadiazole)s (POD) present a well-combined properties such as good strength/stiffness, fatigue resistance, and low density, which makes these polymers competitive in performance when compared to other engineering plastics [15].

In order to obtain polymer nanocomposites with high relative permittivity along with low losses, for the first time we have manufactured sulfonated POD (sPOD)-based nanocomposite films with 0.2-10.0 wt% graphene sheets via solution mixing and casting, and have investigated their electrical and dielectric properties as functions of frequency of 20 Hz-2 MHz. For the purpose, graphene sheets as nanoscale fillers have been prepared by acid-treatment of natural graphite and following thermal expansion. In addition, the molecular interaction and microstructural features of sPOD/graphene nanocomposite films are characterized by using FT-IR spectroscopy, electron microscopy, and X-ray diffraction method.

Experimental

Materials

sPOD with weight-average molecular weight of ~80,000 g/mol, which was synthesized from dicarboxylic acid 4,4-diphenylether (DPE, >99 %, Sigma-Aldrich) and hydrazine sulfate (HS, >99 %, Sigma-Aldrich), was used as polymeric

*Corresponding author: ygjeong@cnu.ac.kr

matrix [16]. Natural graphite flake with average diameter of ~500 μm was purchased from Sigma-Aldrich, Inc. Nitric acid (HNO_3, 60 %) and sulfuric acid (H_2SO_4, 90 %) were purchased from Junsei Chemical Co., Ltd. Potassium chlorate ($KClO_3$, 99.5 %) was obtained from Kanto Chemical. Co., Ltd. Exfoliated graphene sheets as a reinforcing nano-scale filler for sPOD was manufactured by the oxidation of the natural graphite using a mixed $HNO_3/H_2SO_4/KClO_3$ solution and the following rapid thermal expansion at 1050 °C for 30 sec [17-19]. Dimethyl sulfoxide (DMSO, >98 %, Samchun Chemical) was adopted for a solvent for preparing sPOD/graphene solution mixtures.

Preparation of sPOD and sPOD/graphene Nanocomposite Films

A series of sPOD-based nanocomposite films containing different graphene contents of 0.1-10.0 wt% were fabricated by ultrasonication-assisted solution mixing and casting, as can be seen schematically in Figure 1. Firstly, predetermined amounts of graphene sheets (0.1-10.0 wt% of sPOD) were dispersed and ultrasonicated in DMSO for 3 hrs. Secondly, sPOD was added into graphene/DMSO solutions, which were then ultrasonicated at 80 °C for 5 hrs. Thirdly, each sPOD/graphene/DMSO solution was casted into a petri-dish on a hot plate at 70 °C for 12 hrs to evaporate DMSO solvent. Finally, to remove any residual solvent, the films were immersed in a water at 60 °C for 24 hrs and dried in a vacuum oven at 120 °C for 24 hrs. The thickness of the films was controlled to be ~80 μm. The final nanocomposite samples were coded as sPOD/G_x, where x indicates the graphene content in the nanocomposite films by wt%. As a reference, a neat sPOD film was also prepared by the same procedure.

Characterization

The molecular structure and interaction of the neat sPOD and its nanocomposite films with containing different graphene contents were characterized by using a FT-IR spectrometer (Nicolet iS10, Thermo Scientific). To identify the dispersion state of the graphene sheets in the nanocomposite films, the cross-section morphology of the films was examined using a transmission electron microscope (JEM-2100, JEOL). For TEM experiments, the nanocomposite films were cryo-sectioned with aid of an ultramicrotome (PT-PC&CR-X, Boeckeler Instruments, Inc.). The ordered structure of graphene sheets in the nanocomposite films was characterized by using a high performance X-ray diffractometer (XRD, X-Pert PRO MPD). The electrical and dielectric properties of the nanocomposite films in the frequency range from 20 Hz to 2 MHz were measured at room temperature with aid of an impedance analyzer (E4980A, Agilent). The nanocomposite film samples with ~1 cm^2 area, onto which silver electrodes were applied, were tested.

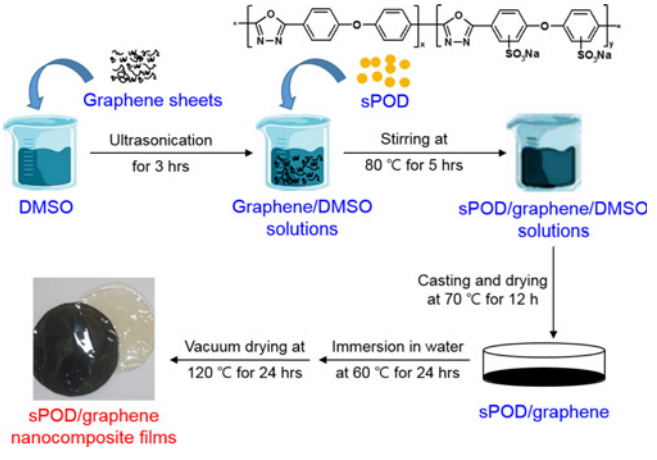

Figure 1. Scheme procedure to manufacture sPOD/graphene nanocomposite films.

Results and Discussion

Structural Characterization

In order to characterize the specific molecular interaction between sPOD and graphene sheets, FT-IR spectra of the neat sPOD and its nanocomposite films containing different graphene contents were obtained, as shown in Figure 2. In case of the neat sPOD, the oxadiazole ring can be characterized by the presence of C=N stretching bands at ~1468 cm^{-1} and ~1415 cm^{-1}, as well as -C-O-C- stretching band at ~1085 cm^{-1}. The C=C stretching bands associated with the aromatic groups of sPOD were observed at ~1600 cm^{-1} and ~1488 cm^{-1} [16,20]. The asymmetric and symmetric SO_2 stretching vibration bands are also observed at 1415-1308 cm^{-1} and 1234-1145 cm^{-1}, respectively, and the asymmetric and symmetric SO stretching vibration bands are detected at 1027-859 cm^{-1} and 837-670 cm^{-1}, respectively. On the other hand, it should be mentioned that the bands at ~1488 cm^{-1} and ~1468 cm^{-1} for the neat sPOD, which are associated with C=C and C=N stretching, was slightly shifted to ~1483 cm^{-1} and ~1464 cm^{-1} for the sPOD/G_10.0 film, respectively, which strongly supports the presence of π-π interaction between aromatic rings of sPOD and graphene sheets in the nanocomposite films.

Figure 3 shows X-ray diffraction patterns of sPOD, graphene sheets, and their nanocomposite films. For the neat sPOD and graphene sheets, there was no diffraction peaks associated with crystalline or ordered structures. It means that the neat sPOD film is purely amorphous and the graphene sheets, which were manufactured by the acid-treatment of the crystalline graphite flake and following thermal expansion, are totally exfoliated. In cases of the nanocomposite films with low graphene contents of 0.1-0.3 wt%, no specific diffraction peak was observed. On the other hand, the nanocomposite films with high graphene contents of 0.7-10.0 wt% exhibited a weak and broad

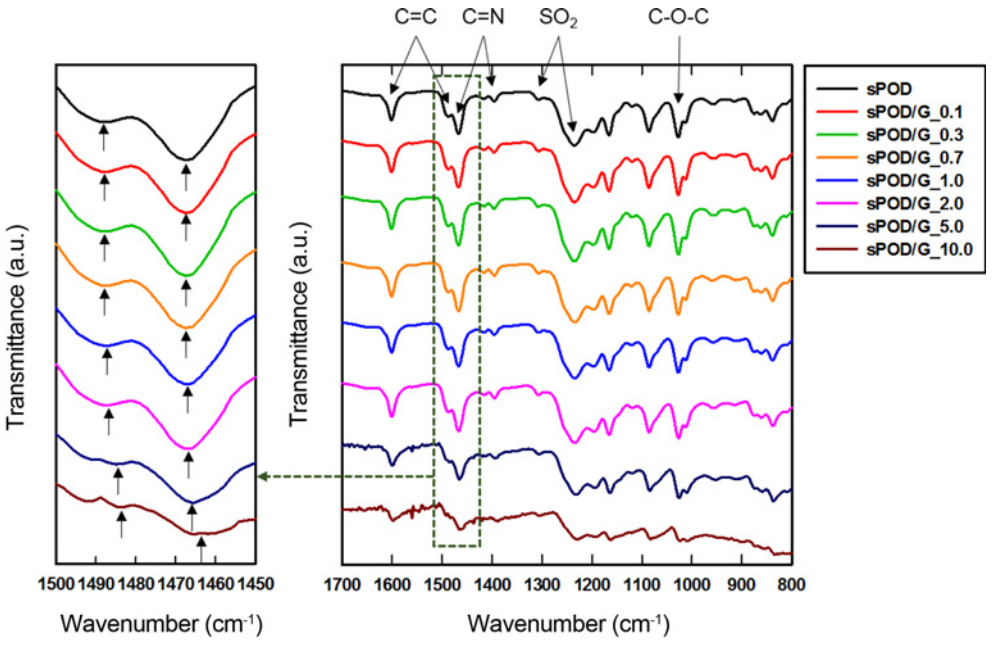

Figure 2. FT-IR spectra of the neat sPOD and its nanocomposite films with different MWCNT contents.

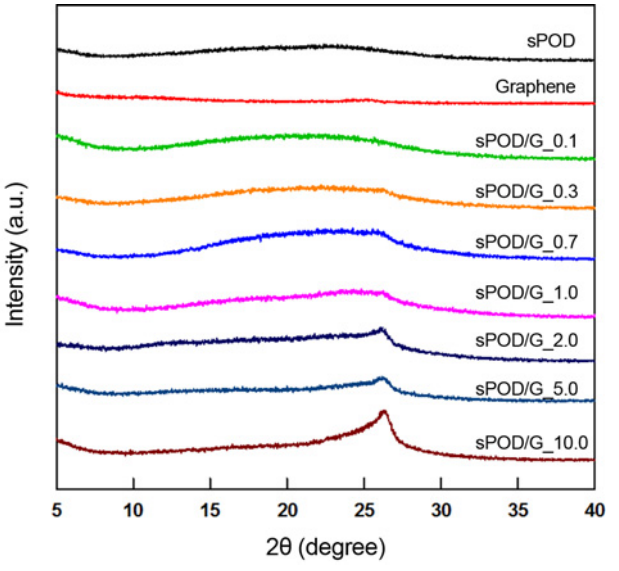

Figure 3. X-ray diffraction patterns and of sPOD, graphene, and their nanocomposite films with different graphene content.

diffraction peak at ~26° corresponding to the *d*-spacing of 0.36 nm, which is associated with the inter-distance among the graphene sheets dispersed laterally in the nanocomposite films of ~80 μm thickness. In addition, the diffraction peak at ~26° became intense with the increment of the graphene content in the nanocomposite films. This result demonstrates that 2-dimensional graphene sheets could form a layered structure in relatively thin nanocomposite films of ~80 μm thickness.

TEM image of the sPOD/G_10.0 film confirmed that the graphene sheets were dispersed but oriented perpendicularly to thickness direction of the nanocomposite film without forming interconnected network structure (Figure 4(A)), although the graphene sheets are well exfoliated and laminated from the crystalline natural graphite via the acid-treatment and thermal expansion process (Figure 4(B)). From the above structural analysis of sPOD/graphene nanocomposite films, it is reasonable to contend that 2-dimensional conductive graphene sheets are dispersed in a series configuration by the presence of insulating sPOD matrix, as illustrated in Figure 4(C). Thus it is conjectured that the laterally aligned structure of graphene sheets will influence strongly the electrical and dielectric properties of the nanocomposite films.

Electrical Property

Figure 5(A) shows the electrical conductivity of the neat sPOD and its nanocomposite films with various graphene contents in the frequency range from 20 Hz to 2 MHz. It was found that the electrical conductivity of the nanocomposite films was strongly dependent on the graphene content as well as the applied frequency. For the neat sPOD and nanocomposite films with 0.2-2.0 wt% graphene, the electrical conductivity was measured to be ~10^{-13}-10^{-12} S/cm at 20 Hz and it increased with the increment of the frequency. This low electrical conductivity as well as its increasing trend with the applied frequency demonstrates that the neat sPOD and its nanocomposite films with 0.2-2.0 wt% graphene are electrically insulating. In case of the sPOD/G_5.0 film, electrical conductivity was in the order of ~10^{-9} S/cm at

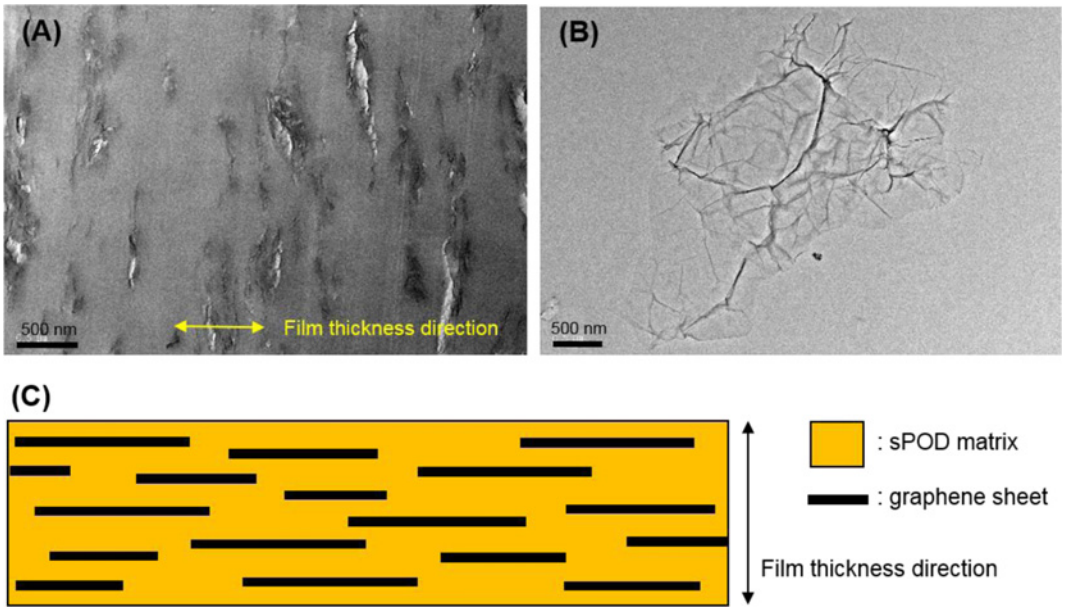

Figure 4. TEM images of (A) graphene sheet and (B) sPOD/G_10.0, and (C) schematic drawing of microstructure for sPOD/graphene nanocomposite films.

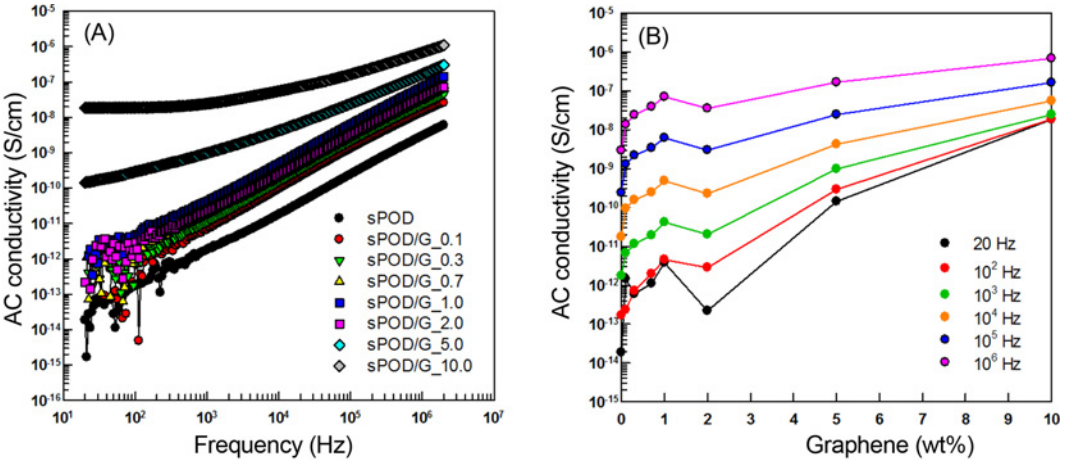

Figure 5. (A) frequency-dependent electrical conductivity and (B) graphene content-dependent electrical conductivity of sPOD and its nanocomposite films with different graphene contents.

20 Hz and then it increased with increasing the frequency by reaching up to ~10^{-6} S/cm at 2 MHz. On the other hand, for the sPOD/G_10.0 film, electrical conductivity was very close to ~10^{-7} S/cm and the value increased slightly to ~10^{-5} S/cm with the variation of the electric field frequency.

The change of electrical conductivity of the nanocomposite films at different constant frequencies as a function of the graphene content is presented in Figure 5(B). The electrical conductivity increased noticeably with the increment of the graphene content in the nanocomposite film, which was dominant at lower applied frequency. The relatively low electrical conductivity of ~10^{-9}-10^{-6} S/cm at 20 Hz for the nanocomposite films with high graphene contents of 5.0 and 10.0 wt% are associated with the structural features of graphene sheets, which are layered but separated in the nanocomposite films, as discussed above. It is thus suggested that electron charges cannot transport efficiently though the conductive graphene sheets dispersed in the nanocomposite films [21]. It has been recently reported that, for the efficient electrical conduction in graphene-based polymer composites via the electron hopping mechanism, the distance between graphenes in the nanocomposites should be smaller than the maximum tunneling distance of electrons, which is evaluated to be ~1.8 nm [22]. Therefore, it is considered that the distance

between graphene sheets in the nanocomposites with even high graphene contents of 5.0-10.0 wt% is not close enough for electrons to hop among graphene sheets. Nonetheless, it is worthy to note that the electrical conductivity of ~10^{-9}-10^{-6} S/cm at 20 Hz for the nanocomposite films with 5.0-10.0 wt% is high enough to be used for electrostatic dissipation (ESD) application [23].

Dielectric Property

In general, the dielectric material as a capacitor may not be an ideal insulator, because the capacitor is not associated with a pure capacitance, but is also related with a resistance. Thus, the non-ideal capacitor includes effectively both a capacitor and a resistor. Therefore, the sPOD/graphene nanocomposite films, where graphene sheets are surrounded by insulating sPOD matrix, manufactured in this study can be considered as non-ideal capacitors. Since the response of materials to alternating electric fields is characterized by a relative permittivity, it is natural to separate its real and imaginary parts, which is expressed by convention in the following way:

$$\varepsilon_r(\omega) = \frac{\varepsilon(\omega)}{\varepsilon_0} = \varepsilon_r'(\omega) + i\varepsilon_r''(\omega) \quad (1)$$

where, $\varepsilon(\omega)$ is the complex frequency-dependent absolute dielectric permittivity, ε_0 is the vacuum permittivity, ε_r' is the real part of the relative permittivity complex, which is related to the stored energy within the medium, ε_r'' is the imaginary part of the relative permittivity, which is related to the dissipation (or loss) of energy within the medium, and ω is the applied frequency.

For sPOD-based nanocomposite films with various graphene contents, changes of relative permittivity, $\varepsilon_r(\omega)$, with the applied electric field frequency from 20 Hz to 2 MHz were examined at room temperature, as shown in Figure 6. Relative permittivity of the neat sPOD and its nanocomposite films with low graphene content of 0.2-2.0 wt% was in the range of 1.7-6.6 at 20 Hz, which was higher for the nanocomposite films with higher graphene content, and it decreased slightly to 1.3-6.0 at 2 MHz. In case of the nanocomposite with 5.0 wt% graphene, the relative permittivity of ~100.9 at 20 Hz decreased logarithmically to ~4.2 at 2 MHz. For the nanocomposite with 10.0 wt% graphene, a high relative permittivity decreased with the increment of the applied frequency from ~560.2 at 20 Hz to 11.6 at 2 MHz. As described above, it was identified that each graphene sheet, which was surrounded by insulating sPOD chains, was dispersed in layers in the nanocomposite. It is

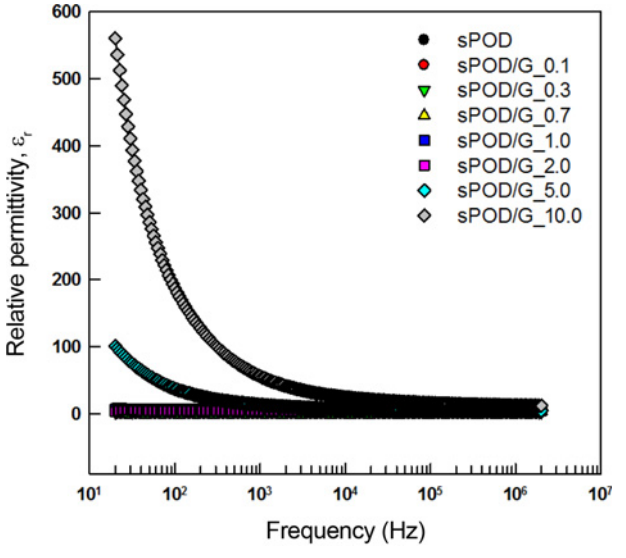

Figure 6. Relative permittivity of sPOD and its nanocomposite films with different graphene contents as a function of frequency.

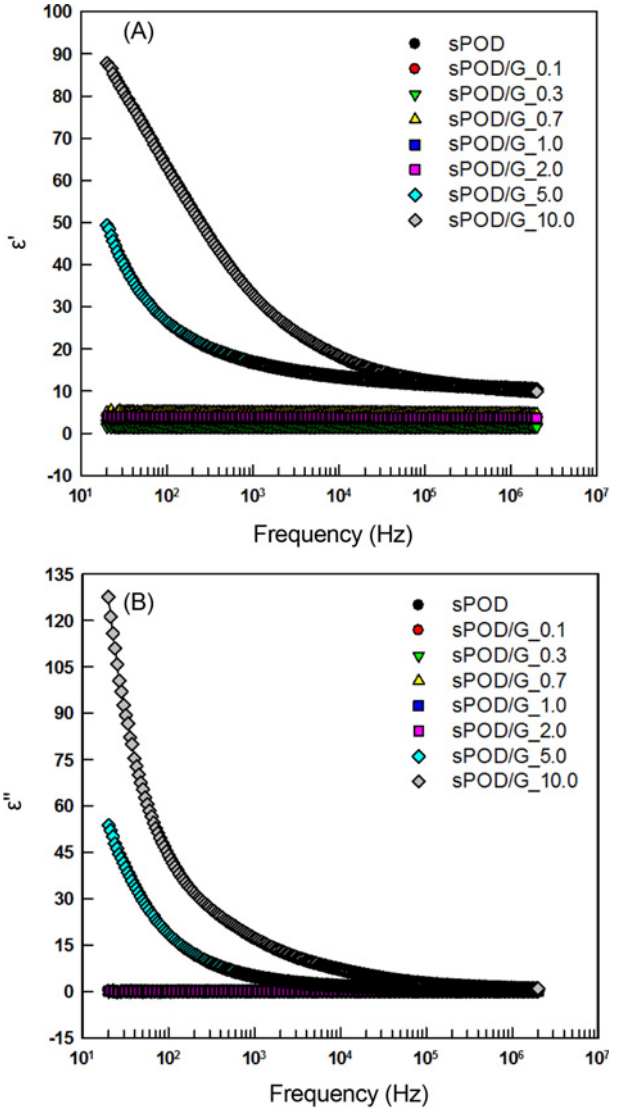

Figure 7. (A) Storage permittivity and (B) loss permittivity of sPOD and its nanocomposite films with different graphene contents as a function of frequency.

generally accepted that the relative permittivity is a measure of the ability of a material to be polarized by an electric field. According to the Maxwell-Wagner polarization effect, charges can be accumulated at the interface between two dielectric materials with different relaxation times given by τ (= ε/σ, where ε is the dielectric permittivity and σ is the electrical conductivity) when current flows across the interface between two materials [24]. Therefore, it is supposed that the high relative dielectric permittivity of ~560.2 at 20 Hz for the nanocomposite with 10.0 wt% graphene is associated with the electronic charge accumulation at the interfaces between conductive graphene sheets and insulating sPOD matrix.

Figure 7(A) and (B) shows changes of the real and imaginary parts, ε_r' and ε_r'', of the relative permittivity of the neat sPOD and its nanocomposite films with 0.1-10.0 wt% graphene as a function of the frequency. For the neat sPOD and nanocomposite films with low graphene contents of 0.1-2.0 wt%, both low ε_r' and ε_r'' values remained constant over the frequency range. However, for the nanocomposite films with high graphene contents of 5.0 and 10.0 wt%, both ε_r' and ε_r'' values decreased significantly with the increment of the frequency. It should be notable that the imaginary permittivity for the nanocomposite films with 5.0 and 10.0 wt% at 20 Hz were higher than the real permittivity. This result is considered to be caused by the partial dissipation of electric energy within the nanocomposite films with high graphene contents of 5.0-10.0 wt%.

Capacitance is the ability of a material to store an electrical charge. In a parallel plate capacitor as a common form of energy storage device, capacitance is directly proportional to the surface area of the conductor plates and inversely proportional to the separation distance between the plates. In addition, the capacitance is a function only of the geometry (including their distance) of the conductors and the permittivity of the dielectric. Figure 8 shows the changes of capacitance of sPOD and its nanocomposites with different graphene contents in the frequency range from 20 Hz to 20 MHz. For the neat sPOD and its nanocomposite films with 0.1-2.0 wt% graphene, the capacitance was in the range of 5-11 pF, which was not dependent on the applied frequency. In cases of the nanocomposite films with 5.0 and 10.0 wt% graphene, relatively high capacitances of ~39.7 pF and ~75.5 pF were attained at 20 Hz, respectively, and they decreased with the increment of the applied frequency. This result supports that the electrical charges can be accumulated easily at the interfaces between conductive graphene sheets and insulating sPOD matrix at low frequency, but the charges are easily dissipated at high frequency, which is consistent with the above results on frequency-dependent electrical and dielectric performance.

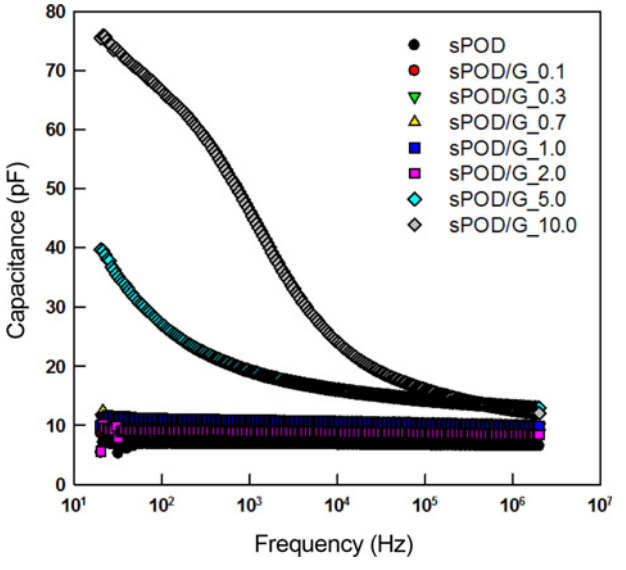

Figure 8. Capacitance of sPOD and its nanocomposite films with different graphene contents as a function of frequency.

Conclusion

In the present study, a series of sPOD-based nanocomposite films with graphene contents of 0.1-10.0 wt% were manufactured by ultrasonication-based solution mixing and casting, and their electrical and dielectric properties in the frequency range from 20 Hz to 2 MHz were investigated, in combination with the microstructural analysis. FT-IR spectra exhibited the presence of specific interaction between sPOD and graphene sheets. TEM images of sPOD/graphene nanocomposite films confirmed that graphene sheets were dispersed in layers by wrapped with sPOD chains. Accordingly, the frequency-dependent electrical conductivity and dielectric permittivity of the nanocomposite films were strongly dependent on the graphene content. For the neat sPOD and its nanocomposites with low graphene contents of 0.1-2.0 wt%, the electrical conductivity increased steadily from ~10^{-13}-10^{-12} S/cm to ~10^{-8}-10^{-7} S/cm with increasing the frequency, while the relative permittivity of 1.3-6.6 remained almost unchanged over the frequency range. In case of nanocomposite with 5.0 wt% graphene, relatively high electrical conductivity of ~10^{-9} S/cm at 20 Hz increased to ~10^{-6} S/cm at 2 MHz, and high dielectric permittivity of ~100.9 at 20 Hz was measured. On the other hand, for the nanocomposite film with 10.0 wt% graphene, the huge dielectric permittivity of ~560.2 at 20 Hz was achieved and it decreased to ~11.6 at 2 MHz, although electrical conductivity of ~10^{-7} S/cm at 20 Hz increased to ~10^{-5} S/cm at 2 MHz. It was interpreted that the huge dielectric permittivity for the nanocomposite with 10.0 wt% graphene stemmed from the charge accumulation at interfacial layers between insulating sPOD chains and conductive graphene sheets dispersed in layers. Accordingly, the nanocomposite films with 5.0 and 10.0 wt exhibited relatively high capacitances of ~39.7 pF and ~75.5 pF at 20 Hz, respectively. Overall, it is conjectured that sPOD-

based nanocomposite films with high graphene contents could be applied for electro-mechanical actuators or renewable chargers as well as electrostatic dissipation materials.

Acknowledgment

This work was supported by the National Research Foundation of Korea (NRF) Grant funded by the Korean Government (MOE) (2013R1A1A2A10010080).

References

1. Z.-M. Dang, J.-K. Yuan, J.-W. Zha, T. Zhou, S.-T. Li, and G.-H. Hu, *Prog. Mater. Sci.*, **57**, 660 (2012).
2. Y. Wu, X. Lin, X. Shen, X. Sun, X. Liu, Z. Wang, and J.-K. Kim, *Carbon*, **89**, 102 (2015).
3. M. Arbatti, X. Shan, and Z. Cheng, *Adv. Mater.*, **19**, 1369 (2007).
4. J.-R. Yoon, J.-W. Han, K.-M. Lee, and H.-Y. Lee, *Trans. Electr. Electron. Mater.*, **10**, 116 (2009).
5. A. K. Geim and K. S. Novoselov, *Nature Mater.*, **6**, 183 (2007).
6. A. A. Balandin, S. Ghosh, W. Z. Bao, I. Calizo, D. Teweldebrhan, F. Miao, and C. N. Lau, *Nano Lett.*, **8**, 902 (2008).
7. C. Lee, X. Wei, J. W. Kysar, and J. Hone, *Science*, **321**, 385 (2008).
8. J. Campos-Delgado, Y. A. Kim, T. Hayashi, A. Morelos-Gomez, M. Hofmann, H. Muramatsu, M. Endo, H. Terrones, R. D. Shull, M. S. Dresselhaus, and M. Terrones, *Chem. Phys. Lett.*, **469**, 177 (2009).
9. I.-H. Kim, D. H. Baik, and Y. G. Jeong, *Macromol. Res.*, **20**, 920 (2012).
10. D. Wang, Y. Bao, J. W. Zha, J. Zhao, Z. M. Dang, and G. H. Hu, *ACS Appl. Mater. Interfaces*, **4**, 6273 (2012).
11. S. H. Hsiao and J. H. Chiou, *J. Polym. Sci. Pol. Chem.*, **39**, 2271 (2001).
12. E. Hamciuc, M. Bruma, T. Köpnick, Y. Kaminorz, and B. Schuz, *Polymer*, **42**, 1809 (2001).
13. S. Janietz and S. Anlauf, *Macromol. Chem. Phys.*, **203**, 427 (2002).
14. D. Gomes, J. Roeder, M. L. Ponce, and S. P. Nunes, *J. Power Sources*, **175**, 49 (2008).
15. H. C. Bach, F. Dobinson, K. R. Lea, and J. H. Saunders, *J. Appl. Polym. Sci.*, **23**, 2125 (1979).
16. E. Lee and Y. G. Jeong, *Compos. Pt. B-Eng.*, **77**, 162 (2013).
17. L. Staudenmaier, *Ber. Dtsch. Bot. Ges.*, **31**, 1481 (1898).
18. H. C. Schniepp, J.-L. Li, M. J. McAllister, H. Sai, M. Herrera-Alonso, D. H. Adamson, R. K. Prudhomme, R. Car, D. A. Saville, and I. A. Aksay, *J. Phys. Chem. B.*, **110**, 8535 (2006).
19. M. J. McAllister, J.-L. Li, D. H. Adamson, H. C. Schniepp, A. A. Abdala, J. Liu, M. Herrera-Alonso, D. L. Milius, R. Car, R. K. Prudhomme, and I. A. Aksay, *Chem. Mater.*, **19**, 4396 (2007).
20. M. R. Loos, V. Abetz, and K. Schulte, *J. Polym. Sci. A Polym. Chem.*, **48**, 5172 (2010).
21. Z. Wang, J. K. Nelson, H. Hillborg, S. Zhao, and L. S. Schadler, *Adv. Mater.*, **24**, 3134 (2012).
22. E. T. Thostenson, C. Li, and T.-W. Chou, *Compos. Sci. Technol.*, **65**, 491 (2005).
23. M. Moniruzzaman and K. I. Winey, *Macromolecules*, **39**, 5194 (2006).
24. R. Tamura, E. Lim, T. Manaka, and M. Iwamoto, *J. Appl. Phys.*, **100**, 114515 (2006).